Kato's theorem and ultralong-range Rydberg molecules

Matthew T. Eiles [*] and Frederic Hummel [†]

Max Planck Institute for the Physics of Complex Systems, Nöthnitzer Str. 38, 01187 Dresden, Germany

We consider nonadiabatic coupling in the "trilobite"-like long-range Rydberg molecules created by perturbing degenerate high-ℓ Rydberg states with a ground-state atom. Due to the flexibility granted by the high Rydberg level density, the avoided crossings between relevant potential energy curves can become extremely narrow, leading to highly singular nonadiabatic coupling. We find that the gap between the trilobite potential curve and neighboring "butterfly" or "dragonfly" potential curves can even vanish, as in a conical intersection, if the gap closes at an internuclear distance which matches a node of the s-wave radial wave function. This is an unanticipated outcome of Kato's theorem.

I. INTRODUCTION

Nonadiabatic physics in the context of ultracold Rydberg atoms has garnered increased interest in recent years. In long-range Rydberg molecules, the coupling between potential wells capable of supporting vibrational levels and dissociative potential curves has been investigated as a possible decay mechanism [1–4]. Theoretical and experimental work has shown that nonadiabatic coupling can become strong enough to induce nonperturbative shifts in vibrational binding energies [5–7]. In cold or ultracold Rydberg collisions, the available chemical reaction pathways for molecular formation, state-changing collisions, or ionization are often determined by the strength of nonadiabatic coupling parameters [4,8–10]. Interacting Rydberg ions [11,12] and Rydberg aggregates [13–16] have been proposed as systems with which to probe and control dynamics through conical intersections.

An ultralong-range Rydberg molecule consists of a Rydberg atom with principal quantum number n and a distant (located $R \sim n^2 a_0$ away) "perturber" atom in its electronic ground state. Nonadiabatic physics are a particularly interesting aspect of this system due to the close connection between the potential energy curves and the Rydberg wave functions [17–20]. Additionally, the large size of the molecules makes them an ideal laboratory to explore beyond Born-Oppenheimer physics on exaggerated scales, and the flexibility provided by Rydberg state parameters allows for controllable enhancement or suppression of nonadiabatic effects and the possibility to steer ultracold chemical reactions.

In this article we show how the nodal positions of the Rydberg wave functions can be linked to very strong, even singular, vibronic coupling between the "high-ℓ" or "trilobite"-like states of a ultralong-range Rydberg molecule. This effort extends previous work [8] which showed that singular nonadiabatic coupling can arise in apparent contradiction of the von Neumann–Wigner no-crossing rule [21]. We find an unexpected connection between these conical intersections and the spatial generalization of Kato's theorem [22] derived by March [23]. Kato's theorem first emerged in the context of density functional theory and quantum chemistry [24–27]. It relates the total electron density at the origin to its spatial derivative through $\partial \rho(r)/\partial r|_{r=0} = -2\rho(0)$. March showed that this cusp condition is a limiting case of a general expression $\partial \rho(r)/\partial r = -2\rho_s(r)$, valid for a bare Coulomb potential, where $\rho_s(r)$ is the s-state density at any position r. This was also discovered in the calculation of electron transfer in charged particle collisions [28–30]. In the following we prove that the coupling between some of the adiabatic potential curves of a Rydberg molecule is proportional to $\partial \rho/\partial r$, and thus Kato's theorem guarantees that this coupling can sometimes vanish.

II. THEORY

The interaction between the two atoms composing a Rydberg molecule is mediated by the rapidly moving Rydberg electron (at position $\boldsymbol{r}$), which only encounters the short-ranged forces from the perturber (at position $\boldsymbol{R}$) inside of a small volume centered on it. Across this region the Coulomb potential is essentially flat, and the electron-perturber interaction potential $\hat{V}(\boldsymbol{r}, \boldsymbol{R})$ is spherically symmetric with respect to the perturber. It is therefore conveniently described by an expansion into partial waves L defined with respect to the perturber. The S-wave contribution to this interaction is the well-known Fermi pseudopotential [31]. The contribution of each partial wave is determined by the electron-perturber scattering phase shift $\delta_L(k)$, which depends on the internuclear distance through the semiclassical

———————
[*]meiles@pks.mpg.de

[†]Present address: Atom Computing, Inc., Berkeley, CA 94710; frederic@atom-computing.com

momentum $k \equiv k(\boldsymbol{R}, n) = \sqrt{2/|\boldsymbol{R}| - 1/n^2}$ (here, and throughout, we use atomic units). These phase shifts scale as $\delta_L(k) \sim \frac{k^2}{L^3}$ for $L \geqslant 2$ and, since $k \ll 1$, the importance of higher-order partial waves decreases rapidly [32–34]. Hence, in the general theory developed below for the adiabatic potential energy curves $U_K(\boldsymbol{R})$, we give particular expressions only for the $N = 3$ most relevant partial waves, $L = 0, 1, 2$ [35]. The molecular states are denoted "trilobite," "butterfly," and "dragonfly," respectively [33,35]. To keep the algebra transparent, we assume $0 < \delta_L(k) < \pi$.[1]

We obtain the set of adiabatic potentials $U_K(\boldsymbol{R})$ by solving the electronic Schrödinger equation:

$$[\hat{H}_e(\boldsymbol{r}) + \hat{V}(\boldsymbol{r}, \boldsymbol{R})]\chi^K(\boldsymbol{r}; \boldsymbol{R}) = U_K(\boldsymbol{R})\chi^K(\boldsymbol{r}; \boldsymbol{R}). \quad (1)$$

Although $\hat{V}(\boldsymbol{r}, \boldsymbol{R})$ is described using electronic partial waves L defined with respect to the perturber, a natural basis to expand $\chi^K(\boldsymbol{r}; \boldsymbol{R})$ into is the eigenstates of $\hat{H}_e(\boldsymbol{r})$. These are the Rydberg states $\phi_{n\ell m}(\boldsymbol{r}) = \frac{u_{n\ell}(r)}{r} Y_{\ell m}(\hat{r})$ with angular momentum $0 \leqslant \ell \leqslant n - 1$ relative to the ionic core. As the diatomic system possesses cylindrical symmetry, each m can be treated individually and we consider just $m = 0$ below. The adiabatic eigenstates are therefore written $\chi^K(\boldsymbol{r}; \boldsymbol{R}) = \sum_\ell \psi_\ell^K(\boldsymbol{R})\phi_{n\ell 0}(\boldsymbol{r})$ in this basis.

As our focus here lies on the high-ℓ states, we neglect the quantum defects $\mu_\ell = \delta_\ell/\pi$ caused by deviations from a pure Coulomb potential in a nonhydrogenic atom. We additionally neglect coupling to additional n levels. Both of these assumptions[2] are well justified here [20,36] and permit the replacement of $\hat{H}_e(\boldsymbol{r})$ by the number $E_n = -1/(2n^2)$ and the development of analytic expressions. In the following we define all such energies relative to E_n. The adiabatic potential curves $U_K(\boldsymbol{R})$ are obtained by diagonalizing $\hat{V}$, whose matrix elements in the degenerate ℓ subspace of a given n are[3]

$$V_{\ell\ell'} = -\sum_{L=0}^{N-1} W_{\ell L}^\dagger W_{L\ell'}. \quad (2)$$

$V_{\ell\ell'}$ shows how the interaction with the perturber causes an incoming Rydberg electron with angular momentum ℓ (relative to the ionic core) to scatter, via each partial wave L (relative to the perturber), into a state ℓ'. The first three rows of the rectangular matrix $W_{L\ell}$ are given in Appendix A. We solve the eigenvalue problem $\sum_{\ell'} V_{\ell\ell'} \psi_{\ell'}^K(\boldsymbol{R}) = U_K(\boldsymbol{R}) \psi_\ell^K(\boldsymbol{R})$ to obtain the adiabatic potential curves.

---

[1]In all alkali atoms, this condition holds everywhere except small R. This assumption can be relaxed at the expense of more careful algebra involving the imaginary square roots in the β_L terms defined in Appendix A.

[2]An exception occurs when one of the low-ℓ states lies energetically close to the bottom of the trilobite potential. This occurs, for example, in Cs, which has an s-state quantum defect of 4.05. For Rb, the most commonly used alkali atom in Rydberg molecule experiments, the inclusion of quantum defects has a very small effect on the size of the avoided crossing.

[3]Throughout, although in principle all variables defined here depend on n, we keep this dependence implicit except at the level of the hydrogen wave functions or energies.

III. NONADIABATIC COUPLING

The strength of the nonadiabatic coupling between adiabatic states K and K', quantified by the derivative coupling matrix $\langle \chi^K | \partial_R \chi^{K'} \rangle$, is inversely proportional to the energy gap $U_K(R) - U_{K'}(R)$. After diagonalizing $\hat{V}$, regions in the potential curves where nonadiabatic coupling becomes large can be identified by searching for small gaps. As pointed out in Ref. [8], these can become arbitrarily small when they occur at a discrete n value close to the position of a conical intersection in the potential surfaces defined as functions of R and n, where n is taken to be a *continuous variable*.

To predict the positions (R_0, n_0) of such conical intersections, it proves essential to represent the interaction operator in a different basis, namely, the *perturber spherical basis* composed of the nonorthogonal states:

$$\tilde{\phi}_L(\boldsymbol{r}; \boldsymbol{R}) = \sum_{L'} [\underline{W}\, \underline{W}^\dagger]_{LL'}^{-1/2} \sum_\ell W_{L'\ell} \phi_{n\ell 0}(\boldsymbol{r}). \quad (3)$$

The transformation from the Rydberg basis to this one is accomplished using the left-inverse matrix $\underline{S}$ satisfying

$$\underline{S} = (\underline{W}\, \underline{W}^\dagger)^{-1/2} \underline{W}, \quad \underline{S}\, \underline{S}^\dagger = \underline{1}_{N \times N}. \quad (4)$$

Using these definitions, it is straightforward to show that $\underline{V} = \underline{S}^\dagger \underline{S}\, \underline{V}\, \underline{S}^\dagger \underline{S}$ [36], and thus the eigenvalue equation determining the potential energy curves is written

$$\sum_{L'} \tilde{V}_{LL'}(\boldsymbol{R}) \tilde{\psi}_{L'}^K(\boldsymbol{R}) = U_K(\boldsymbol{R}) \tilde{\psi}_L^K(\boldsymbol{R}), \quad (5)$$

where $\tilde{\psi}_L^K = \hat{\sum}_\ell S_{L\ell} \psi_\ell^k$, $\tilde{V}_{LL'} = \sum_{\ell, \ell'} S_{L\ell} V_{\ell\ell'} S_{\ell'L'}^\dagger = -\sum_\ell W_{L\ell} W_{\ell L'}^\dagger$, and $\chi^K(\boldsymbol{r}; \boldsymbol{R}) = \sum_L \tilde{\psi}_L^K(\boldsymbol{R}) \tilde{\phi}_L(\boldsymbol{r}; \boldsymbol{R})$ in this representation. The matrix element $\tilde{V}_{LL'}$ is proportional to the overlap $\langle \tilde{\phi}_L | \tilde{\phi}_{L'} \rangle$, computed explicitly in Appendix A. Clearly, rather than dealing with the $n \times n$ matrix $\underline{V}$ of Eq. (2), it suffices to study the conditions necessary to obtain degenerate eigenvalues of the $N \times N$ matrix $\underline{\tilde{V}}$. A semiclassical approximation for the elements $\tilde{V}_{LL}$, first derived by Borodin and Kazansky (BK) [37,38], is

$$\tilde{V}_{LL}(R) \approx U_L^{\text{BK}} \equiv \frac{1}{2n^2} - \frac{1}{2(n - \delta_L(k)/\pi)^2}. \quad (6)$$

IV. TRILOBITE-BUTTERFLY SUBSPACE

We first consider the subspace with $L \leqslant 1$, corresponding to the trilobite and butterfly states. The 2×2 matrix $\underline{\tilde{V}}$ possesses degenerate eigenvalues if $\tilde{V}_{00} = \tilde{V}_{11}$ simultaneously as $\langle \tilde{\phi}_0 | \tilde{\phi}_1 \rangle = 0$. That the latter condition can be met is not guaranteed *a priori*: the overlaps determining the diagonal elements, for example, are nodeless [see Eqs. (B1) and (B2)]. However, employing the spatial generalization of Kato's cusp theorem [27], we obtain

$$\langle \tilde{\phi}_0 | \tilde{\phi}_1 \rangle = -|\phi_{n00}(\boldsymbol{R})|^2. \quad (7)$$

This result, that the coupling between trilobite and butterfly states is determined by the hydrogenic s-wave probability density alone, shows that the coupling vanishes when
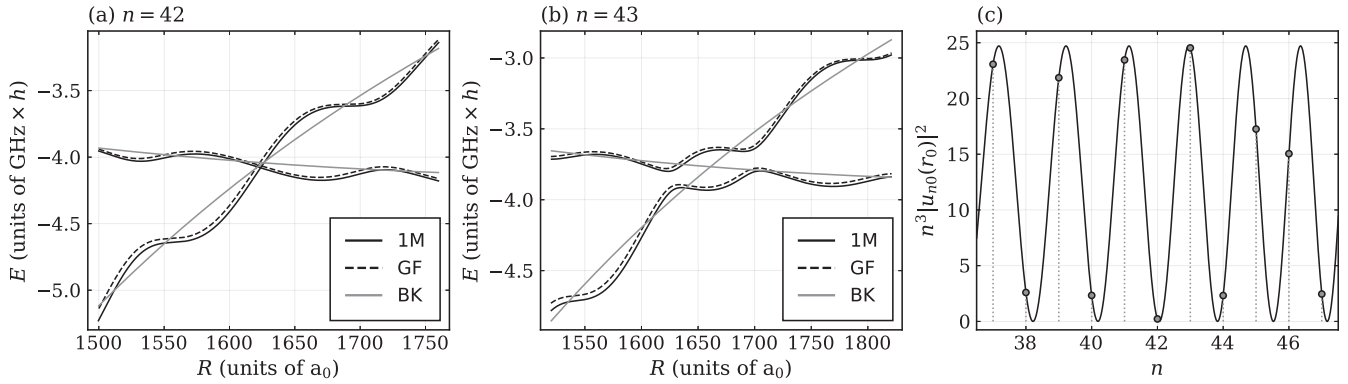
$$u_{n0}(R) = 0, \quad (8)$$

FIG. 1. Crossings of the adiabatic potential energy curves at principal quantum numbers $n = 42$ (a) and $n = 43$ (b). The solid curves (1M) show the numerical eigenvalues of $V_{\ell\ell'}$, which involves a single manifold of Rydberg states. The dashed curves (GF) show potential curves obtained via the Green's function method, which includes contributions from all n levels. The two methods agree very closely, especially regarding the size of the avoided crossing. Energies are measured with respect to E_n. The thin gray curves (BK) show the semiclassical potentials U_L^{BK}. As discussed in the text, the very narrow avoided crossing in panel (a) occurs very close to the intersection of these curves. (c) Nodes of the Rydberg $\ell = 0$ orbital. The plotted curve is $n^3|u_{n0}(r_0)|^2$, where r_0 is obtained by solving $k^2 = 2/r_0 - 1/n^2$ for the k value where $\delta_S(k) = \delta_P(k)$. When this function is zero, a conical intersection occurs. Narrow avoided crossings appear when a conical intersection occurs very close to an integer n.

and therefore degenerate eigenvalues are possible. Using the semiclassical result of Eq. (6), we find the first condition, that the diagonal elements are equal, to occur when

$$\delta_L(k) = \delta_{L'}(k) \tag{9}$$

for arbitrary L and L'. For S and P partial waves, if Eqs. (7) and (8) hold at the same (R, n) tuplet, the two partial waves locally decouple and the potential surfaces will cross in a conical intersection. Remarkably, inserting Eq. (8) into the quantum formulas for the diagonal energies [Eqs. (A2), (B1), and (B2)] shows that Eq. (9) holds for the fully quantum calculation as well. That the semiclassical condition perfectly matches the quantum one is another surprising conclusion stemming from Kato's theorem.

Figure 1 shows two extreme examples of the curve crossing between S and P states, using Rb as a perturber and H as the Rydberg atom. The adiabatic potential curves obtained from diagonalizing $\hat{V}$ are shown as solid lines; since this calculation involves only states from a single Rydberg manifold, we label them "1M". For $n = 42$ [Fig. 1(a)] the R value where Eq. (9) holds lies almost perfectly at a node of $u_{42,0}(R)$ [compare Fig. 1(c)]. For $n = 43$ [Fig. 1(b)] this point lies nearly at an antinode of the $n = 43$ wave function. Therefore the former case exhibits an extremely narrow crossing (on the sub-MHz level) while the latter case possesses a pronounced avoided crossing. To confirm that this behavior is not exaggerated by or an artifact of the single-manifold approximation, we performed a numerical Green's function (GF) calculation as well [33,39,40] (dashed curves), which includes contributions from the entire Rydberg spectrum [41]. These two methods agree almost perfectly, especially regarding the existence and size of the narrow avoided crossing, validating the single-manifold approximation, which is at the core of the analytical formulas we derived. We also show the semiclassical curves of Eq. (6), highlighting the fact that these intersect extremely close to the avoided crossing in panel (a).

V. DRAGONFLY CONTRIBUTIONS

We now include the effect of $L = 2$ partial waves. The coupling between S and D,

$$\langle \tilde{\phi}_0 | \tilde{\phi}_2 \rangle \propto \frac{u_{n0}(R)}{4\pi R^3}[2u_{n0}(R) - R u'_{n0}(R)], \tag{10}$$

is also oscillatory. It vanishes when $u_{n0}(R) = 0$ or $\frac{d}{dR} \ln u_{n0}(R) = \frac{2}{R}$. When the former condition holds, the S partial wave decouples from both P and D waves simultaneously. Unfortunately, the algebra of higher L values becomes very tedious [32,42]. We speculate that this decoupling of the S state persists even for higher L values, but further effort is needed to make this generalization rigorous. A degeneracy in the 2×2 subspace of S and D levels is also possible, occurring when the expression in Eq. (10) vanishes simultaneously as $\delta_2(k) = \delta_0(k)$. This semiclassical condition, unlike the SP case, coincides with the quantum condition only in the large-R limit [Eq. (B4)].

Surprisingly, the coupling between P and D states does not oscillate [Eq. (B10)], and therefore these curves *cannot* cross. It is intriguing that, just as Kato's theorem shows the special role played by the s-wave function (defined with the origin at the Rydberg ion), it shows how the S-wave molecular state, defined with the origin at the perturber, also behaves in a nongeneric way.

VI. DISCUSSION

We showed that the $L = 0$ trilobite state decouples from the $L = 1, 2$ partial waves whenever Eq. (8) is satisfied. This is a direct result of Kato's theorem. It is particularly intriguing since the weight of the $\ell = 0$ state in the eigenstates $|\tilde{\psi}_0\rangle$ and $|\tilde{\psi}_1\rangle$ is almost negligible. If the S and P-wave phase shifts are equal when Eq. (8) holds, a conical intersection exists, and its presence will be felt as a nearly exact crossing in the potential curves of nearby integer n levels. Such a conical intersection cannot occur between butterfly and dragonfly potential curves.

It is interesting to contrast these results with what was observed in Ref. [8] for the crossing of a trilobite state with a "low-ℓ" state having with angular momentum ℓ_0 and a nonzero quantum defect μ_{ℓ_0}. Semiclassically, the relevant potential curves become degenerate when

$$\pi \mu_{\ell_0} = \delta_S(k), \tag{11}$$

at the same (R_0, n_0) as $u_{n_0 \ell_0}(R_0) = 0$. Equation (11) resembles Eq. (9) but now requires the phase accumulated by the scattering off of the nonhydrogenic core of the Rydberg atom to match that accumulated from the scattering off of the perturber. This is closely connected with the fact that the R-dependent scattering phase shifts play the role of quantum defects in the Rydberg formula given by Eq. (6). The second condition is analogous to Eq. (8) but differs in a key way which again illustrates the counterintuitive message of Kato's theorem. For a quantum defect state, it is that radial wave function which must possess a node. This carries a certain degree of physical intuition, as this state is the dominant component of one of the electronic states in the system. On the other hand, for the trilobite and butterfly state interaction, there is nothing in the scattering problem or in the pure Coulomb interaction to single out a specific ℓ. However, because Kato's theorem places fundamental importance on $\ell = 0$, this is the state which matters in the end, in what appears to be a surprising accident of the Coulomb potential.

VII. OUTLOOK

The existence of extremely narrow avoided crossings at serendipitous n values could play a crucial role in the behavior of Rydberg atoms in dense background gases, since the various transition probabilities between electronic states determines which decay pathways are available for different collisions [4]. Recently it was proposed that a series of highly diabatic transitions followed by a final adiabatic transition is necessary for the surprising observation that a Rydberg impurity creates a hole in the surrounding condensate density [43]. In both of these contexts, the fact that large deviations from "generic" behavior can occur at anomalous n values should certainly be considered. More broadly, Rydberg molecules could provide a physical realization of the type of bound state in the continuum predicted in Ref. [44]. It would be interesting to see if similar physics can be discovered in long-range Rydberg polyatomic molecules of the type considered in Refs. [45–47], where the ground-state atom is replaced by a dipolar molecule. Although the interaction between the electron and the molecule is very different from the atom-electron potential, the resulting potential curves resemble those studied here, suggesting there might exist similar behavior in their avoided crossings. This would also address the more general question of the importance of a zero-range potential, rather than a finite-ranged potential, on the size of avoided crossings. Finally, further exploration of the high-L states to test our hypothesis that they all similarly decouple from the S state would be interesting if the challenging algebra of high-L pseudopotentials could be treated in an elegant way [32,42].

APPENDIX A: MATRIX ELEMENTS OF $\tilde{V}$

The $L \leqslant 2$ matrix elements of the $N \times n$ rectangular matrix $\underline{W}$ are

$$W_{0\ell} = \beta_0 \, \phi_{n\ell 0}(\boldsymbol{R}) \tag{A1a}$$

$$W_{1\ell} = \beta_1 \frac{\partial}{\partial R} \phi_{n\ell 0}(\boldsymbol{R}) \tag{A1b}$$

$$W_{2\ell} = \beta_2 \left(\frac{3}{2} \frac{\partial^2}{\partial R^2} + \frac{k^2}{2} \right) \phi_{n\ell 0}(\boldsymbol{R}), \tag{A1c}$$

where $\beta_L = \sqrt{2(2L+1)\pi k^{-(2L+1)} \tan \delta_L(k)}$. The matrix elements of $\tilde{V}$ are

$$\tilde{V}_{LL'} = -\beta_L \beta_{L'} \tilde{Q}_{LL'}, \tag{A2}$$

where

$$\tilde{Q}_{LL'} = Q_{LL'}, \ L, L' \leqslant 1, \tag{A3a}$$

$$\tilde{Q}_{L2} = \tfrac{1}{2}(3Q_{L2} + k^2 Q_{L0}), \ L \leqslant 1, \tag{A3b}$$

$$\tilde{Q}_{22} = \tfrac{1}{4}(9Q_{22} + 6k^2 Q_{20} + k^4 Q_{00}). \tag{A3c}$$

These formulas make use of the quantity

$$Q_{\alpha\beta} = \sum_{\ell=0}^{n-1} \sum_{m=-\ell}^{m=\ell} \frac{\partial^{\alpha}}{\partial R^{\alpha}} \phi_{n\ell m}^*(\boldsymbol{R}) \frac{\partial^{\beta}}{\partial R^{\beta}} \phi_{n\ell m}(\boldsymbol{R}). \tag{A4}$$

APPENDIX B: COMPUTED Q VALUES

In Appendix A, the matrix $\tilde{\underline{V}}$ is defined in terms of the overlap matrix $\tilde{\underline{Q}}$, which is in turn defined using $Q_{\alpha\beta}$ [Eq. (A4)] as a sum over the degenerate ℓ and m states. This summation can be performed analytically, as described in [20,28,29]. In doing so, all $\tilde{Q}$ terms can be defined in terms of only the s-wave radial wave function and its derivative, as summarized below. We use $u \equiv u_{n0}(R)$ and $u' \equiv u'_{n0}(R)$ to shorten the notation:

$$\tilde{Q}_{00} = \frac{1}{4\pi}[k^2 u^2 + u'^2] \tag{B1}$$

$$\tilde{Q}_{11} = \frac{k^2}{3} Q_{00} - \frac{1}{6\pi R^2} \left(2uu' - \frac{u^2}{R} \right) \tag{B2}$$

$$\tilde{Q}_{22} = \frac{1}{20\pi n^2 R^3} \left[\frac{2n^4(2R+9) + R^3 - 4n^2 R^2}{n^2} u'^2 \right.$$
$$+ \frac{4(n^2(2R-9) - R^2)}{R} uu' + 4(2-3R)u^2$$
$$\left. + \frac{6n^2 R^4 - R^5 + (18 + R(8R-7))n^6}{n^4 R^2} u^2 \right]. \tag{B3}$$

For $R \gg 1$,

$$\tilde{Q}_{22} \sim \frac{k^2}{20\pi} \left[(ku')^2 + \frac{4}{R^2} uu' + (k^2 u)^2 \right]. \tag{B4}$$

We note here that the expressions given for Q_{11} and a related quantity in Ref. [20] are incorrect. We report the correct formulas here for completeness:

$$\Upsilon_{33} = \frac{4\pi R^2 k^2 Q_{00} - uu' - u^2/R}{12\pi R^2} \tag{B5}$$

$$\Upsilon_{22} = Q_{11} \tag{B6}$$

$$= \Upsilon_{33} - \frac{u_{n0}(R)}{4\pi R^3}(Ru' - u). \tag{B7}$$

For large n values the missing term does not lead to noticeable differences. The various off-diagonal couplings are

$$\tilde{Q}_{01} = -|\phi_{n00}(R))|^2 = -\frac{u^2}{4\pi R^2} \tag{B8}$$

$$\tilde{Q}_{02} = \frac{u}{4\pi R^3}[2u - Ru'] \tag{B9}$$

$$\tilde{Q}_{12} = -\frac{1}{8\pi R^2}\left[3\left(\frac{u}{R} - u'\right)^2 + k^2 u^2\right]. \tag{B10}$$

For completeness, another useful result is

$$Q_{02} = -\frac{k^2}{3}Q_{00} + \frac{1}{6\pi R^2}\left(\frac{2u^2}{R} - uu'\right). \tag{B11}$$

APPENDIX C: GREEN'S FUNCTION

The closed-form Coulomb Green's function [48] leads to a transcendental equation [33,40]

$$0 = A_0(A_1 - A_{01}), \tag{C1}$$

where

$$A_0 = 1 - \Phi_v \frac{\tan\delta_0}{k} \tag{C2}$$

$$A_1 = 1 + (\Phi_{vvv} - 3\Phi_{uuv})\frac{\tan\delta_1}{k^3} \tag{C3}$$

$$A_{01} = \frac{\tan\delta_0/k}{1 - \Phi_v \tan\delta_0/k}3\Phi_{uv}^2\frac{\tan\delta_1}{k^3}, \tag{C4}$$

whose solutions give the potential energy curves $V(R) = -\frac{1}{2\nu(R)}^2$. Here, $\nu(R)$ is the R-dependent principal quantum number whose noninteger part gives the deviation from the unperturbed hydrogen levels caused by the perturber. The various Φ_x terms in Eq. (C1) relate to derivatives of the Coulomb
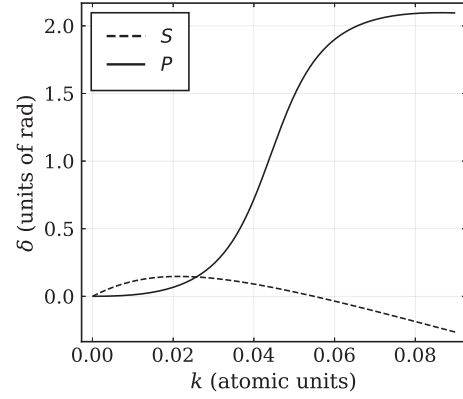

FIG. 2. S- and P-wave phase shifts used to compute Fig. 1, taken from [49].

Green's function. The zeros of A_0 and A_1, computed individually, give the $L = 0$ and $L = 1$ potential curves. A_{01} describes the coupling between these terms and vanishes whenever

$$0 = \Phi_{uv} = -\frac{\nu\Gamma(1-\nu)}{2R^2}M_{\nu,1/2}\left(\frac{2R}{\nu}\right)W_{\nu,1/2}\left(\frac{2R}{\nu}\right), \tag{C5}$$

where M and W are Whittaker functions. When ν is an integer, the nodes of $M_{\nu,1/2}$ and $W_{\nu,1/2}$ coincide with those of u_{n0}, and hence we recover the result from diagonalization discussed in the main text.

APPENDIX D: RUBIDIUM PHASE SHIFTS

The existence of narrow avoided crossings at a specific n value does depend sensitively on the electronic phase shifts, and in particular, on the energy where they are computed to become identical. For reproducibility, we show in Fig. 2 the electron-rubidium scattering phase shifts used in our calculations, which match those of Ref. [49]. For other sets of phase shifts, whether they are computed using different methods or measured experimentally, we would expect the n values where conical intersections nearly occur to differ due to any change in the intersection point.

[1] A. Duspayev and G. Raithel, Nonadiabatic decay of Rydberg-atom–ion molecules, Phys. Rev. A **105**, 012810 (2022).

[2] A. Duspayev, A. Shah, and G. Raithel, Nonadiabatic decay of metastable states on coupled linear potentials, New J. Phys. **24**, 053043 (2022).

[3] J. Deiglmayr, Long-range interactions between Rydberg atoms, Phys. Scr. **91**, 104007 (2016).

[4] M. Schlagmüller, T. C. Liebisch, F. Engel, K. S. Kleinbach, F. Böttcher, U. Hermann, K. M. Westphal, A. Gaj, R. Löw, S. Hofferberth, T. Pfau, J. Pérez-Ríos, and C. H. Greene, Ultracold chemical reactions of a single Rydberg atom in a dense gas, Phys. Rev. X **6**, 031020 (2016).

[5] S. Hollerith, J. Zeiher, J. Rui, A. Rubio-Abadal, V. Walther, T. Pohl, D. M. Stamper-Kurn, I. Bloch, and C. Gross, Quantum

gas microscopy of Rydberg macrodimers, Science **364**, 664 (2019).

[6] R. Srikumar, F. Hummel, and P. Schmelcher, Nonadiabatic interaction effects in the spectra of ultralong-range Rydberg molecules, Phys. Rev. A **108**, 012809 (2023).

[7] F. Hummel, P. Schmelcher, and M. T. Eiles, Vibronic interactions in trilobite and butterfly Rydberg molecules, Phys. Rev. Res. **5**, 013114 (2023).

[8] F. Hummel, M. T. Eiles, and P. Schmelcher, Synthetic dimension-induced conical intersections in Rydberg molecules, Phys. Rev. Lett. **127**, 023003 (2021).

[9] P. Geppert, M. Althön, D. Fichtner, and H. Ott, Diffusive-like redistribution in state-changing collisions between Rydberg atoms and ground state atoms, Nat. Commun. **12**, 3900 (2021).

[10] T. Niederprüm, O. Thomas, T. Manthey, T. M. Weber, and H. Ott, Giant cross section for molecular ion formation in ultracold Rydberg gases, Phys. Rev. Lett. **115**, 013003 (2015).

[11] F. M. Gambetta, C. Zhang, M. Hennrich, I. Lesanovsky, and W. Li, Exploring the many-body dynamics near a conical intersection with trapped Rydberg ions, Phys. Rev. Lett. **126**, 233404 (2021).

[12] M. Magoni, R. Joshi, and I. Lesanovsky, Molecular dynamics in Rydberg tweezer arrays: Spin-phonon entanglement and Jahn-Teller effect, Phys. Rev. Lett. **131**, 093002 (2023).

[13] S. Wüster, A. Eisfeld, and J. M. Rost, Conical intersections in an ultracold gas, Phys. Rev. Lett. **106**, 153002 (2011).

[14] K. Leonhardt, S. Wüster, and J. M. Rost, Switching exciton pulses through conical intersections, Phys. Rev. Lett. **113**, 223001 (2014).

[15] R. Pant, R. Agrawal, S. Wüster, and J. M. Rost, Nonadiabatic dynamics in Rydberg gases with random atom positions, Phys. Rev. A **104**, 063303 (2021).

[16] K. Leonhardt, S. Wüster, and J. M. Rost, Orthogonal flexible Rydberg aggregates, Phys. Rev. A **93**, 022708 (2016).

[17] C. H. Greene, A. S. Dickinson, and H. R. Sadeghpour, Creation of polar and nonpolar ultra-long-range Rydberg molecules, Phys. Rev. Lett. **85**, 2458 (2000).

[18] J. P. Shaffer, S. T. Rittenhouse, and H. R. Sadeghpour, Ultracold Rydberg molecules, Nat. Commun. **9**, 1965 (2018).

[19] C. Fey, F. Hummel, and P. Schmelcher, Ultralong-range Rydberg molecules, Mol. Phys. **118**, e1679401 (2020).

[20] M. T. Eiles, Trilobites, butterflies, and other exotic specimens of long-range Rydberg molecules, J. Phys. B: At. Mol. Opt. Phys. **52**, 113001 (2019).

[21] J. von Neumann and E. P. Wigner, Über merkwürdige diskrete Eigenwerte, Phys. Z. **30**, 467 (1929).

[22] T. Kato, On the eigenfunctions of many-particle systems in quantum mechanics, Commun. Pure Appl. Math. **10**, 151 (1957).

[23] N. H. March, Spatially dependent generalization of Kato's theorem for atomic closed shells in a bare Coulomb field, Phys. Rev. A **33**, 88 (1986).

[24] O. J. Heilmann and E. H. Lieb, Electron density near the nucleus of a large atom, Phys. Rev. A **52**, 3628 (1995).

[25] S. M. Blinder, Sturmian propagator for the nonrelativistic Coulomb problem, Phys. Rev. A **29**, 1674 (1984).

[26] R. Shakeshaft and L. Spruch, Semiclassical evaluation of sums of squares of hydrogenic bound-state wavefunctions, J. Phys. B: At. Mol. Phys. **18**, 1919 (1985).

[27] N. H. March, Bound-state Slater sum for a bare Coulomb field derived from s-states alone, Phys. Lett. A **111**, 47 (1985).

[28] M. Chibisov, A. M. Ermolaev, F. Brouillard, and M. H. Cherkani, New summation rules for Coulomb wave functions, Phys. Rev. Lett. **84**, 451 (2000).

[29] M. H. Cherkani, F. Brouillard, and M. Chibisov, Summation rules for Coulomb wavefunction products, J. Phys. B: At. Mol. Opt. Phys. **34**, 49 (2001).

[30] R. Shakeshaft and L. Spruch, Mechanisms for charge transfer (or for the capture of any light particle) at asymptotically high impact velocities, Rev. Mod. Phys. **51**, 369 (1979).

[31] E. Fermi, Sopra lo spostamento per pressione delle righe elevate delle serie spettrali, Nuovo Cim. **11**, 157 (1934).

[32] A. Omont, On the theory of collisions of atoms in Rydberg states with neutral particles, J. Phys. France **38**, 1343 (1977).

[33] E. L. Hamilton, C. H. Greene, and H. R. Sadeghpour, Shape-resonance-induced long-range molecular Rydberg states, J. Phys. B: At. Mol. Opt. Phys. **35**, L199 (2002).

[34] M. I. Chibisov, A. A. Khuskivadze, and I. I. Fabrikant, Energies and dipole moments of long-range molecular Rydberg states, J. Phys. B: At. Mol. Opt. Phys. **35**, L193 (2002).

[35] P. Giannakeas, M. T. Eiles, F. Robicheaux, and J. M. Rost, Dressed ion-pair states of an ultralong-range Rydberg molecule, Phys. Rev. Lett. **125**, 123401 (2020).

[36] M. T. Eiles, A. Eisfeld, and J. M. Rost, Anderson localization of a Rydberg electron, Phys. Rev. Res. **5**, 033032 (2023).

[37] V. M. Borodin and A. K. Kazansky, The adiabatic mechanism of the collisional broadening of Rydberg states via a loosely bound resonance state of ambient gas atoms, J. Phys. B: At. Mol. Opt. Phys. **25**, 971 (1992).

[38] P. Giannakeas, M. T. Eiles, F. Robicheaux, and J. M. Rost, Generalized local frame-transformation theory for ultralong-range Rydberg molecules, Phys. Rev. A **102**, 033315 (2020).

[39] A. A. Khuskivadze, M. I. Chibisov, and I. I. Fabrikant, Adiabatic energy levels and electric dipole moments of Rydberg states of Rb_2 and Cs_2 dimers, Phys. Rev. A **66**, 042709 (2002).

[40] C. H. Greene and M. T. Eiles, Green's-function treatment of Rydberg molecules with spins, Phys. Rev. A **108**, 042805 (2023).

[41] C. Fey, M. Kurz, P. Schmelcher, S. T. Rittenhouse, and H. R. Sadeghpour, A comparative analysis of binding in ultralong-range Rydberg molecules, New J. Phys. **17**, 055010 (2015).

[42] Z. Idziaszek and T. Calarco, Pseudopotential method for higher partial wave scattering, Phys. Rev. Lett. **96**, 013201 (2006).

[43] F. Engel, S. K. Tiwari, T. Pfau, S. Wüster, and F. Meinert, In situ observation of chemistry in Rydberg molecules within a coherent solvent, arXiv:2308.13762.

[44] L. S. Cederbaum, R. S. Friedman, V. M. Ryaboy, and N. Moiseyev, Conical intersections and bound molecular states embedded in the continuum, Phys. Rev. Lett. **90**, 013001 (2003).

[45] S. T. Rittenhouse and H. R. Sadeghpour, Ultracold giant poly-atomic Rydberg molecules: Coherent control of molecular orientation, Phys. Rev. Lett. **104**, 243002 (2010).

[46] R. González-Férez, H. R. Sadeghpour, and P. Schmelcher, Rotational hybridization, and control of alignment and orientation in triatomic ultralong-range Rydberg molecules, New J. Phys. **17**, 013021 (2015).

[47] R. González-Férez, J. Shertzer, and H. R. Sadeghpour, Ultralong-range Rydberg bimolecules, Phys. Rev. Lett. **126**, 043401 (2021).

[48] L. Hostler and R. H. Pratt, Coulomb Green's function in closed form, Phys. Rev. Lett. **10**, 469 (1963).

[49] F. Engel, T. Dieterle, F. Hummel, C. Fey, P. Schmelcher, R. Löw, T. Pfau, and F. Meinert, Precision spectroscopy of negative-ion resonances in ultralong-range Rydberg molecules, Phys. Rev. Lett. **123**, 073003 (2019).